A characterization of the spray evolution by dual-mode phase doppler anemometry in an injector of liquid-propellant thruster †

Jin Seok Kim[1] and Jeong Soo Kim[2,*]

[1]*Department of Mechanical Engineering, Sunchon National University, Maegok 315, Suncheon, Jeonnam 540-742, Korea*
[2]*School of Mechanical Engineering, Pukyong National University, San 100, Yongdang-dong, Nam-gu, Busan 608-739, Korea*

Abstract

Spray characteristics of an injector employed in the 5 Newton-class of liquid-propellant thruster are addressed with an evolutionary feature of droplets. Information for the droplets is obtained through Dual-mode phase Doppler anemometry (DPDA) measurement in terms of the velocity, diameter, number density, and turbulent intensity. In addition, instantaneous images for the macroscopic view of spray are supplemented by flow visualization technique using laser sheet. It is demonstrated by the investigation of spray images that the injector under consideration meets an angular injection requirement at all of the injection pressures specified. Spray shedding is also featured with a schematization of the frozen images. Dynamic behavior of spray droplets and their atomization evolution along the geometric axis of injector-nozzle orifice with varying injection pressures are scrutinized by depicting the cumulative droplet populations mapped onto a velocity-diameter domain. The evolutionary behavior is further authenticated on the basis of the distribution for number density and turbulent intensity of droplets. It is inferred that the higher injection pressure generates the smaller droplets undergoing the greater deceleration along the spray stream due to the augmented Reynolds number and Weber number. Even though spray characterization of the current type of injectors is to be inevitable to their performance estimation at the design stage, it has never been reported to date. It is expected that the present results will be able to contribute to the appreciation of injector performance and to the design engineering of brand-new thrusters as well.

Keywords: Atomization; Droplet; Dual-mode Phase Doppler anemometry (DPDA); Flow visualization; Liquid-propellant thruster; Spray break-up

---

1. Introduction

Liquid propellant thrusters have been developed and applied to the attitude and velocity control of space vehicles since the earlier stage of the global space era. Particularly, monopropellant thrusters in which hypergolic fuel is directly injected onto catalyst bed have the advantages of low development cost, simple structure, and long/stable propellant storability in the case that low thrust/impulse bits and long sys-

tem-operation time are required. A systematic investigation for the fuel spray generated from thruster injector is indispensable to the design and development of thrust chamber in that thruster performances such as thrust, fuel consumption rate, and impulse bit are significantly affected by the spray behavior inside the chamber. As an effort to evaluate the performance of small liquid-propellant rocket engine, Kim et al. [1] carried out hot-fire tests under vacuum environment and predicted a theoretical performance of the engines as well. During their performance tests, thrust instability phenomenon was noticed, which has been an issue and concern to liquid rocket engines from the earlier development age. By the way, a periodic na-

---

ture of fuel-spray atomization process was previously reported to associate with the combustion instability in liquid rocket engines [2].

Injection performance and spray atomization characteristics for the liquid rocket injector of swirl coaxial type were evaluated by Kenny et al. [3] utilizing the diagnostics of shadowgraph and Phase Doppler particle analyzer (PDPA) for the spray field in a pressurized and optically accessible chamber. In their study, with various representations to classify the atomization regimes by dimensionless parameters, such as Reynolds number, Weber number, and Ohnesorge number, etc., throttling that reduces thrust (or mass flow rates proportional to pressures) with fixed design of combustion chamber resulted in the change of atomization regime. Non-volatile and less hazardous fluids were used in their evaluation as simulants instead of the real and reactive propellants, based on the fact that the injection and primary atomization processes are those generally least affected by the propellant reaction.

Li and Shen [4] studied the characteristics of spray produced from the breakup of annular water jets exposed to inner air stream, simulating twin-fluid atomization, by means of Phase Doppler anemometry (PDA). Spray characteristic parameters composed of the mean diameter, mean velocity, velocity fluctuation, and number density of droplets were measured and derived at various radial and axial locations, indicating that those parameters were almost symmetric about the central axis of spray.

Not only the injection pressure but the internal flow inside an injector nozzle also affects external spray pattern. Koo [5] observed effects of nozzle-inlet shape and operating pressure conditions on the transient fuel-spray behavior in terms of spray characteristic parameters by using PDPA. Influence of geometry on the internal flow and macroscopic spray behavior in diesel nozzle was also examined by Payri et al. [6]. They pointed out that cavitation leads to an increment of the spray cone angle as well as hole-outlet velocity.

An earlier survey for the effects of nozzle configuration on jet atomization was made in detail by Reitz and Bracco [7] along with various length to diameter ratio (l/d) ranging over 0.5 to 85 for sharp and rounded inlets and an exit diameter of $0.34\,mm$. Their experiments showed that, for very small l/d, say less than 2, the exit flow was likely to be influenced by details of the entrance flowfield, nozzle design,

and even nozzle imperfection coming from fabrication.

The single realization condition that there must be only one particle in a measurement (probe) volume at a time is of utmost importance for the droplet size measurement of dense sprays so as to be considered valid and accurate. It can only be met by decreasing the measurement volume size, as examined in detail by Edwards and Marx [8]. On the other hand, the Gaussian beam effect or trajectory effect, which is caused by the condition of volumetric decrease, as recognized by Saffman [9] and outlined further by Gréhan et al. [10] and Sankar et al. [11], leads to larger size errors as the ratio of droplet size to measurement volume diameter increases. Even without altering the measurement volume size, the trajectory effect may well vary significantly in its influence, as a spray evolves downstream through agglomeration [12].

Being motivated by the elimination of the trajectory effect, Tropea et al. [13] explored a new PDA measurement system, which is nowadays called dual-mode PDA (DPDA) with the aim of improving concentration and mass flux measurement. The DPDA is designed in a fashion combining a conventional (or standard) PDA optical arrangement with a planar PDA system. The system is thus believed to eliminate an ambiguity caused by particle trajectory during the size measurement. Recently, comprehensive measurements for the spray droplets exiting from a thruster injector have been conducted by Kim et al. [14] utilizing the DPDA.

To the best of our knowledge, any characterization of the sprays generated from the liquid-propellant thruster injector, which is of a full scale and direct injection type with very small nozzle orifices, has never been performed or reported by others up to date even though it is inevitable to the thruster design and development process. In this paper an experimental setup employing a flow visualization system (FVS) and DPDA is introduced with their constitution and function. Instantaneous images taken by CCD camera of FVS are presented first to macroscopically survey the effects of injection-pressure variation on spray patterns. Additionally, a visual way of inspection for the spray-injection angle of a 5 Newton-class thruster-injector is proposed with the images being examined, as an alternative to using mechanical jig or patternator. Scrutiny into the characteristic spray behavior is made through the quantitative data obtained from DPDA measurement in terms of the mean velocity, mean

diameter, number density, and turbulent intensity of droplets along the spray downstream on an axis of nozzle orifice with varying injection pressures. The population of droplets passing through a measurement volume that is a direct outcome of DPDA measurement is mapped onto a velocity-diameter domain with the evolutionary features of spray being addressed. Categorization of spray-flow regime is made by interrelating the jet Reynolds number and Weber number in order to figure out the atomization and turbulence nature of spray. Spray evolution along with droplets breakup process is schematically illustrated, finally.

2. Experimental setup

The experimental setup is shown in Fig. 1. It comprises the FVS and DPDA system, and the injector-spray generation system whose operational constitution is supplemented in Fig. 2. Deionized water (DIW) pressurized by gaseous nitrogen (GN$_2$), passing through a series of valves and filters is supplied up to injector, and then the injector generates eight (8) spray streams. Because the real hypergolic propellants are normally accompanied by the handling issues of toxicity and explosion safety [15], DIW is used in a laboratory-scale experiment as a simulant that has the liquid properties similar to the propellant of hydrazine (N$_2$H$_4$), as compared in Table 1.

FVS, which captures the instantaneous images of spray, consists of a double-head Nd:Yag laser, cylindrical lens, synchronizer, CCD camera, and a computer. The laser has 120 mJ of maximum pulse power with the pulse duration of 8 ns. The cylindrical lens transforms the laser into a sheet beam. The laser pulses are synchronized with the CCD camera (1280×1024 pixels) equipped with a lens having $f/2.8$ and 600 mm of focal length.

DPDA system which has four-beams for two-velocity components, combining two detectors of a standard PDA system with two detectors of a planar system in a single receiving unit is applied to the current experiment for an accuracy enhancement in droplet size measurement [16]. The system consists of an Ar-Ion laser, transmitter, transmitting probe, receiving probe, detector unit, signal processor, three-dimensional traverse system with stepping motor controller, and a computer for overall system monitoring, surveillance, and control. Output power of the laser (6 W max.) is set to 1 W and is delivered to

Table 1. Comparison of physical properties between H$_2$O and N$_2$H$_4$.

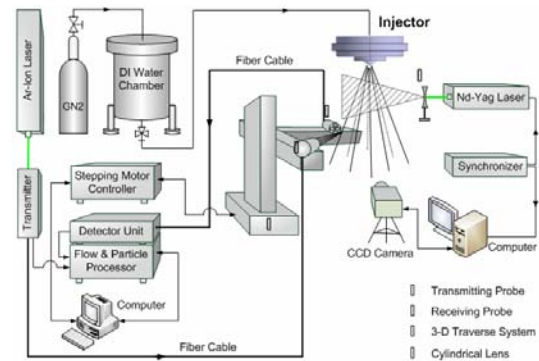|	Melting point [K]	Boiling point [K]	Density [g/ml]	Viscosity [cP]	Surface tension [N/m]
H$_2$O	273.2	373.2	1.00	0.89	72.0x10^{-3}
N$_2$H$_4$	275.2	387.4	1.00	0.91	66.5x10^{-3}

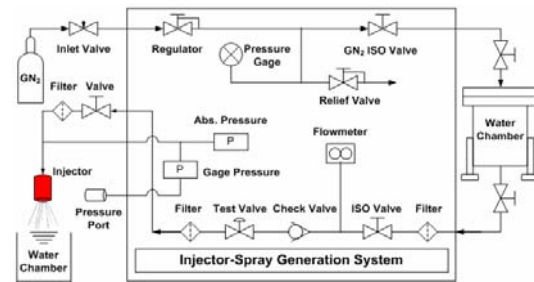Fig. 1. Schematic diagram of the experimental setup.

Fig. 2. Operational constitution of injector-spray generation system.

both the green (514.5 nm) and blue (488 nm) ray components as equally as possible for the same light intensity. The focal length of transmitting probe with an expander and that of receiving probe are 500 mm and 400 mm, respectively. The expander lens with an expansion ratio of 1:1.98 is attached to the front of transmitting probe so as to reduce a size of measurement probe volume.

The measurement volume is formed at the intersection of four laser beams emitted from the transmitting probe, as illustrated in Fig. 3. For the present optical arrangement, dimensions of the measurement volume in each direction are $\delta_x = 0.12$ mm, $\delta_y = 0.12$ mm, and $\delta_z = 1.55$ mm, respectively. When a droplet particle passes through the fringes inside the measurement volume, photomultipliers in
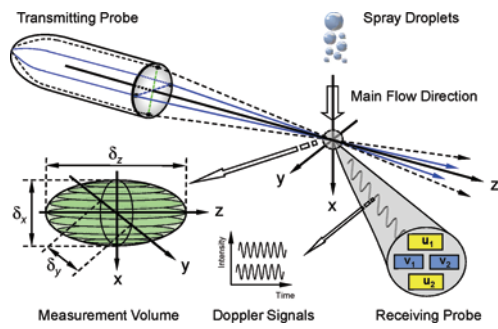
Fig. 3. Formation of measurement probe volume in DPDA.

a detector unit produce uniform Doppler bursts. A phase difference occurs between these bursts due to the slight difference in collection angles among the different detectors. The Doppler signals are analyzed to indicate information on the velocity and size of each particle. In general, the number of samples has great influence on the ensemble-averaged values. It is well known that the sampling number is to be more than 5,500 at a given location for the local mean droplet properties to be guaranteed highly accurate [17]. In line with the previous works, 10,000 droplets with 10 seconds set to the upper limit of acquisition duration are sampled and processed in the present measurement.

Data acquisitions along the spray stream on a geometric axis of nozzle orifice are conducted by sweeping the measurement volume with the aid of 3-dimensional traverse system which has $12.5\,\mu m$ of stepping resolution and $40\,\mu m$ of repeatability. As depicted in Fig. 4, sweeps are sequentially carried out with $5.5\,mm$ of traversing step through forty-one (41) locations away from the orifice exit face.

Configuration of the thruster injector employed in this study is shown in Fig. 5 along with an identification numbering for 8 orifice holes. The axis of each orifice has $30°$-canted angle off from the axis of injector face. Each orifice hole has a length to diameter ratio (l/d) of 1.67, where $l = 0.254$ and $d = 0.152$ (refer to Fig. 4). The orifice is so small in diameter that it cannot be drill-machined but can be holed only by electrical discharge machining (EDM). On the other hand, the EDM does not produce that good quality of geometric consistency among the orifices even in an injector. An enlarged picture of some holes taken by video microscope is presented in Fig. 6. The inter-orifice inconsistency of microscopic configuration is to disrupt the uniformity in spray patterns, as will be revealed in the following section.
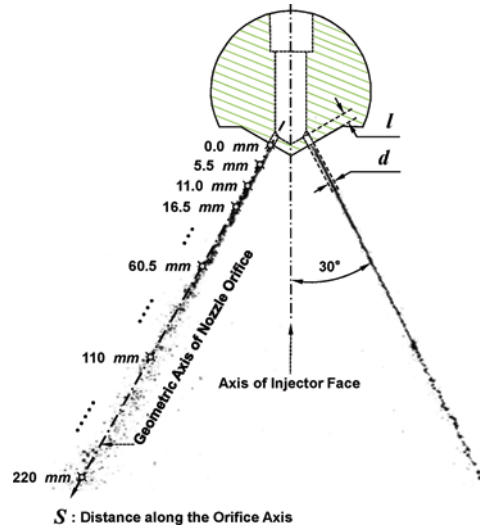

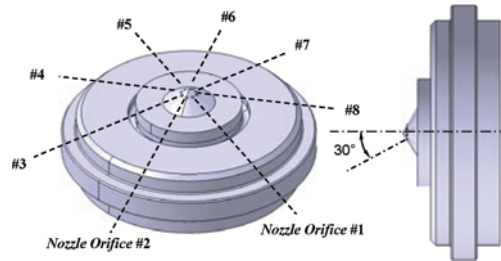Fig. 4. Positional indication for the measurement-volume sweeps along the geometric axis of nozzle orifice.

Fig. 5. Configuration of the injector employed in the experiment.

(a) Nozzle Orifice #1, #2, and #3

(b) Detailed inlet image of *Nozzle Orifice* #3

Fig. 6. Video-microscope images of orifice holes.

3. Results and discussion

Instantaneous spray images were taken by the CCD camera in FVS setup at eight different levels of DIW-supply pressure ranging from 3.4 to $27.6\,bar$ (in gage pressures) with an increment of $3.4\,bar$, where fuel-injection performance of thruster injectors is to be evaluated for their hardware acceptance. Fig. 7 shows the images captured from *Nozzle Orifice* #1 through to #4 . An obtuse triangle with its vertex
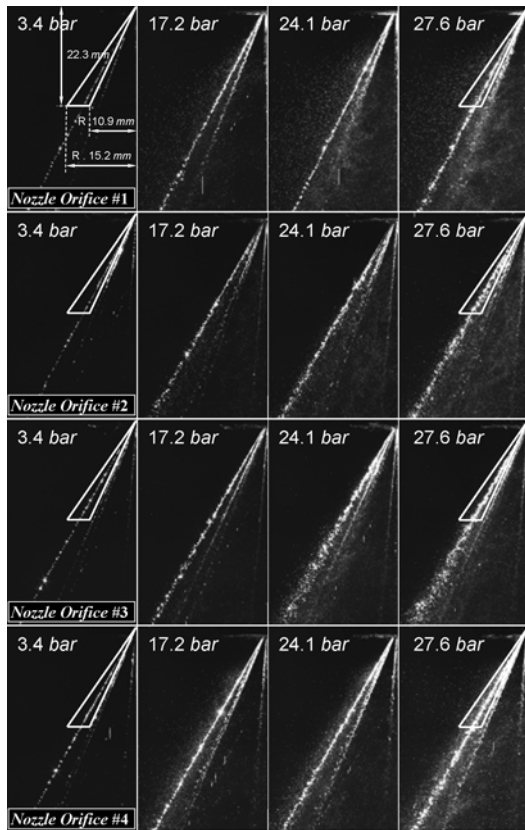
Fig. 7. Instantaneous spray images captured from the respective nozzle orifices with varying pressure.

Fig. 8. Enlarged view of the frozen image taken from *Nozzle Orifice* #3 spray at 27.6 *bar* (leftmost) along with its skeletonizing process for a shedding schematic.

being positioned at the orifice-exit face is overlapped on each image of 3.4 *bar* and 27.6 *bar*. The triangle is a geometrical representation stipulating a pass-fail criterion when the injector head assembly of thruster is put to a water-flow-test for the verification of injection-angle performance: the pass condition is that any lateral dispersion of fuel spray shall be limited to within the triangular region. Therefore, it can be judged from the figure that the thruster injector under consideration satisfactorily meets the injection-angle requirement at all pressure levels, though not every image captured was shown in the figure. Also, it is generally seen that the degree of atomization becomes higher as the pressure increases for all nozzle orifices, whereas atomization patterns are not all the same among the orifices: this looks more apparent at the higher pressures. The difference in atomization patterns is caused by the lack of similarity among the orifice shapes. As was mentioned formerly with Fig. 6, the dissimilarity has its origin in the EDM-fabrication of nozzle orifices which led to microscopic variations
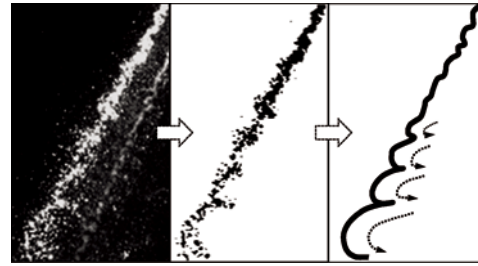
of the inside configuration. Similarly, previous studies indicated that the generation of turbulence, cavitation, and subsequent atomization of liquid jet would be strongly affected by the nozzle inlet geometry as well as the location and configuration of injection orifice [7, 18-21].

Typically, the liquid jet emanating from an injector orifice outlet does start with liquid ligaments and ends up with atomized through a transient region. Likewise, the upper half (or thereabout) in each image of Fig. 7 can be considered pertaining to the liquid ligament region with the lower one regarded as the transient region taking precedence of an atomization maturity to occur at the far downstream. It can be inferred from phase Doppler anemometry physics that the Doppler signals which are reflected/refracted by such a liquid ligament or by severely deformed shape of droplet would necessarily cause a significant distortion of the phase difference to be used in calculation process of droplet sizing [22]. Hence, it is timely to note that such data as droplet sizes acquired ahead of moderate formation of high-sphericity droplets will be so cumbersome to be counted in particle statistics of phase Doppler anemometry. In fact, DPDA filters out those unwanted data by in-process spherical validation.

Fig. 8 shows an enlarged view of the frozen image taken from *Nozzle Orifice* #3 spray at 27.6 *bar* (leftmost) together with its skeletonizing process for obtaining a shedding schematic of the primary stream. The shedding phenomenon could be caught at all sprays, though there was seen some difference in its pulsation strength. Such pulsation was also observed by Faragó and Chigier [23] in a round liquid jet with coaxial air stream: they concluded that atomization would be always accompanied by a pulsating process even if both the emerging liquid to be atomized and the gas were issuing oscillation-free. From acoustic aspects, the spray shedding can be presumed to relate

to a flow instability and further to a combustion instability [24].

Measurements for the spray variables through DPDA were conducted over the same DIW-pressure range as in the spray-image capturing (i.e., from 3.4 to 27.6 *bar* with an increment of 3.4 *bar*). However, spray characterization is focused hereinafter on the pressures greater than 17.2 *bar* because any considerable atomization within the measurement position of concern could not be noticed at the pressures less than that. Fig. 9 shows variation of droplet mean-velocities along the sprays of *Nozzle Orifice* #2 and #3 . With 27.6 *bar* of injection pressure, droplet velocity for both sprays decreases from approximately 62 *m/s* around the orifice exit down to 30 *m/s* at 220 *mm* downstream. The decrease is attributed to the continuous loss of droplet momentum to the surrounding air. The velocity data obtained near the orifice exit region (within 16.5 *mm* from the exit) have not been taken into account in linear curve-fit
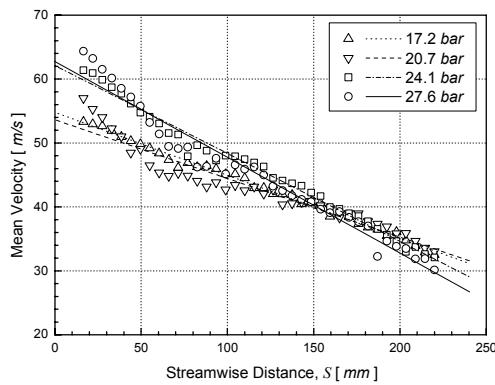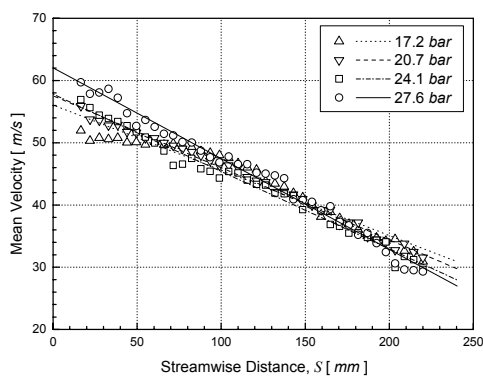
due to the lack of reliability caused by the erroneous Doppler signals originating from liquid ligaments, as noted prior.

The higher the injection pressure (or DIW-supply pressure, though not exactly same) is, the greater the spray velocity should be. This looks clear and is also observable in the upstream region of spray. However, this proportional dependency of velocity on the pressure diminishes as the spray evolves toward downstream, and reverses eventually resulting in the lower droplet velocity at the higher injection pressure: e.g., the droplets injected with 27.6 *bar* decelerate so quickly that the velocity at the far downstream gets even lower than those generated with 17.2 *bar* . The deceleration seems dependent upon the degree of atomization that is a strong function of the injection pressure. A partial deviation from this overall tendency of velocity reversal is witnessed over upstream region of the *Nozzle Orifice* #2 at 20.7 *bar* . With the measurement made along not any center-line of spray but the geometric axis of nozzle orifice being reminded, it may be ascribed to somewhat asymmetrical nature of spray that is caused inherently by the orifice configuration and at the specific pressure endowed.

For the validation of velocity data acquired by DPDA, the injection velocity ($V_{inj,DPDA}$) predicted at the orifice exit by extrapolating DPDA data along the spray stream is compared to that obtainable on the basis of the volume flow rate directly measured. In Fig. 10, $V_{inj,DPDA}$ was deduced from the linear-extrapolation curves of Fig. 11 in which DPDA-velocities are linear-fitted and then averaged over the sprays of *Orifice* #1 to #4 at the respective injection pressures. Practical injection velocities can be calculated by Eq. (1),

(a) Nozzle Orifice #2

(b) Nozzle Orifice #3

Fig. 9. Effect of pressure variation on the mean velocity distribution along spray stream.
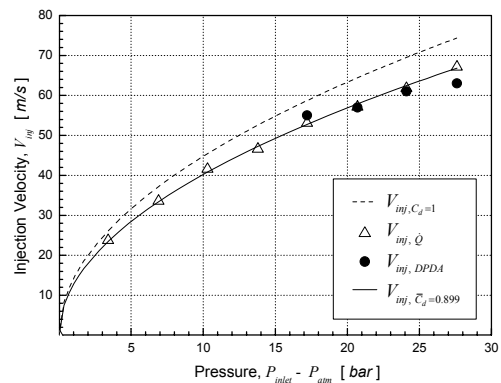
Fig. 10. Validation of the injection velocities acquired by DPDA.

Table 2. Volume flow rate measured with varying injection pressures for the determination of discharge coefficients.

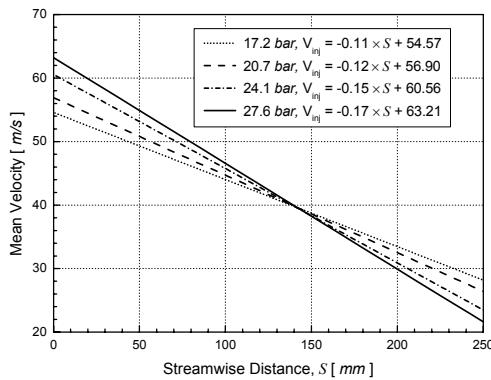| $P_{inlet} - P_{atm}$ [bar]	3.4	6.9	10.3	13.8	17.2	20.7	24.1	27.6
$\dot{Q}_{inj}$ [ml/min]	26.0	36.8	45.5	51.0	58.3	62.5	67.6	73.5
C_d	0.9038	0.9033	0.9132	0.8864	0.9036	0.8869	0.8885	0.9033

Fig. 11. Orifice-averaged (over the *Orifices* #1, #2, #3, and #4) mean-velocity distribution of sprays with varying injection pressures.

$$V_{inj,Q} = \frac{4\dot{Q}_{inj}}{\pi d^2} \qquad (1)$$

where $\dot{Q}_{inj}$ and d indicate the volume flow rate and orifice diameter. Table 2 summarizes the volume flow rate measured with varying injection pressures and the discharge coefficient C_d estimated by the following relationship:

$$C_d = \frac{4\dot{Q}_{inj}}{\pi d^2} \sqrt{\frac{\rho_w}{2(P_{inlet} - P_{atm})}} \qquad (2)$$

where ρ_w, P_{inlet}, and P_{atm} represent water density, DIW-supply pressure onto the injector (in absolute), and atmospheric pressure, respectively. An injection velocity-to-pressure variation with $\overline{C}_d = 0.899$ ($V_{inj,\overline{C}_d}$) that is the discharge coefficient averaged all over the injection pressures is also delineated in Fig. 10: $\overline{C}_d = 0.899$ is comparable to the typical ones reported with the orifice configurations similar to current type [25] although the exact values depend upon the geometry details (e.g., length-diameter ratio, orifice inlet and inside configuration, etc.). The ideal velocities $V_{inj,C_d=1}$ with $C_d = 1$ are necessarily above any others because the irreversible dissipation factors in internal flow and liquid jet are neglected in the calculation adopting the Bernoulli equation. Conclusively, a rationale for the DPDA-velocity measurement accuracy is established based on the orifice-exit
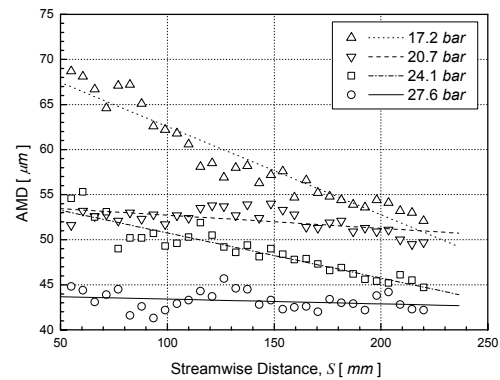
(a) Nozzle Orifice #2
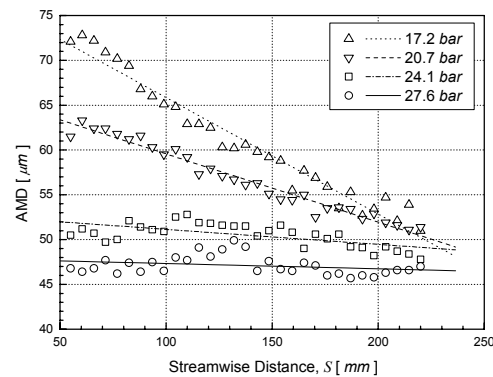
(b) Nozzle Orifice #3

Fig. 12. AMD distribution along the spray stream with varying injection pressures.

values differing by within 6% of those estimated by the volume flow rate.

Variations in arithmetic mean diameter (AMD) of droplets along the axis of nozzle orifice are viewed in Fig. 12 for two nozzle orifices. The absolute AMD values differ slightly from orifice to orifice, but the downsizing tendency along the spray stream and also with increasing injection pressures are similar to each other. For both orifices, the lower injection pressure results in the initiation of larger droplets. With 17.2 *bar*, about 70 μm of AMD at 60 *mm* away from orifice exit does go down to about 52 μm at 220 *mm* downstream. This streamwise reduction rate shrinks as the injection pressure goes up: there cannot

be found any prominent AMD variation at $27.6 \, bar$, after all.

The AMD dependency on injection pressure is inherently relevant to the droplet deceleration along the stream, as was discussed with Fig. 9. With exposure to ambient air, the smaller droplets formed by the finer-atomization at the higher injection pressure rapidly decelerate due to their low mass and inertia suffering an aerodynamic drag. The larger droplets having relatively high inertia are less affected by the surrounding air and thus experience less velocity decrease along the stream. Consequently, it can be inferred to the droplet dynamics in current type of injector sprays that the higher injection pressure generates the smaller droplets undergoing the greater decrease rate of velocity along the spray stream.

An additional remark is needed that the droplet size information from the orifice face up to about $50 \, mm$ downstream was not included in Fig. 12 because the prevalence of liquid ligaments over the region had caused an unrealistic outcome of size via erroneous Doppler signals, as mentioned analogously as in Fig. 7. Processed data over the region showed a streamwise growth of droplet size, which would not be physically possible just except for any occurrences of droplet agglomeration. In general terms, the distance to which the measured AMD is not reliable lessens as the pressure increases owing to the precipitation of high-sphericity droplets passing through a spherical validation process in DPDA.

An auxiliary notation is given in Table 3 for the four representative cases combining pressure levels and probing locations in order to summarize the spray behavior according to pressure variation as well as the streamwise evolution of droplets. Figs. 13 (a) – (d) compare the cumulative population of instantaneous droplets directly measured by DPDA for the four cases in *Nozzle Orifice* #2 spray. For pictorial clarity, values only for 500 droplets among 10,000 samples are mapped onto each velocity-diameter domain. The solid-horizontal and dotted-vertical lines in each domain represent the mean diameter (AMD) and mean velocity, respectively, under the given location and injection pressure. As a whole, all the cases just except for the velocity range in case $C_{L,UP}$ have widely-scattered distributions of droplets in velocity and size. What the case, $C_{L,UP}$ shows a relatively narrow velocity range in the vicinity of $48 \, m/s$ is in line with the fact of insufficient atomization at the upstream under the low injection pressure endowed. Similar observation for the droplets distribution near orifice exit has been reported by Ganippa et al. [18].

An approximate estimation for droplets deceleration along the *Orifice* #2 spray is made in Table 4. Now, macroscopic behaviors of the spray affected by the change of injection pressure can be featured out as follows, with Fig. 13 and Table 4 being referred together:

I. Spray evolution from $C_{L,UP}$ to $C_{L,DW}$: As moving toward downstream, droplets with the mean velocity of about $48 \, m/s$ and the mean diameter of $68 \, \mu m$ whose instantaneous values are ranging so widely from $5 \, \mu m$ through to $170 \, \mu m$, lose

Table 3. Parametric combination defining four (4) *Cases*.

Location, S Pressure, P_{inj}	60.5 mm	220 mm
17.2 bar	$C_{L,\,UP}$	$C_{L,\,DW}$
27.6 bar	$C_{H,\,UP}$	$C_{H,\,DW}$

Table 4. Approximation for droplets deceleration along the *Orifice* #2 spray.

| Measured/Derived Values	Unit	$C_{L,UP}$	$C_{L,DW}$	$C_{H,UP}$	$C_{H,DW}$
Injection pressure (in gage)	bar	17.2		27.6	
Streamwise location	mm	60.5	220.0	60.5	220.0
AMD	μm	68	52	44	42
Mean velocity of droplets	m/s	48.4	32.5	51.4	30.1
Transition distance	m	0.16		0.16	
Vel. change per distance	$(m/s)/m$	-99.7		-133.5	
Ave. vel. per transition	m/s	40.5		40.8	
Elapsed time per transition	s	3.94×10^{-3}		3.91×10^{-3}	
Deceleration	m/s^2	4032		5442	
Deceleration in gravity unit	g	411		555	
Relative change of deceleration	$\%$	0		35	
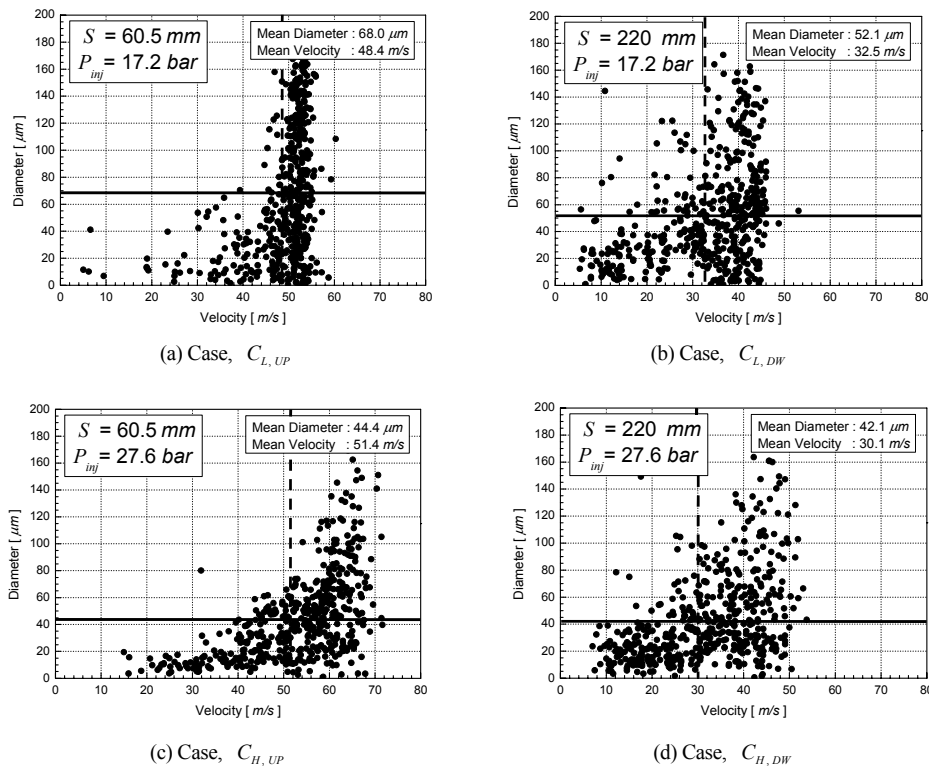
Fig. 13. Cumulative population of instantaneous droplets at the upstream/downstream and with the low/high injection pressures for the *Nozzle Orifice* #2 spray.

their momentum down to $33\,m/s$ and are broken-up to as small as $52\,\mu m$. The break-up and deceleration of droplets originate from their momentum exchange with surrounding air. Velocities of most of the droplets concentrate around the mean values at the upstream, whereas widely disperse at the downstream.

II. $C_{L,UP}$ vs. $C_{H,UP}$: With the elevated injection pressure of $27.6\,bar$, droplet mean velocities get higher ($51\,m/s$) and their instantaneous distribution spreads more widely than at $17.2\,bar$. The velocity spreading as well as the reduced mean droplet size ($44\,\mu m$) implies the more vivid atomization resulted from an interaction of the higher kinetic energy droplets with surrounding air.

III. Spray evolution from $C_{H,UP}$ vs. $C_{H,DW}$: As moving toward downstream with the higher injection pressure, atomization-saturated droplets at the upstream are not severely altered in their sizes, but lose their momentum more rapidly than the situation (I) of lower pressure. It is also observed in this transition that the dense group of high ve-

locity droplets spreads widely over the low-velocity range at the downstream. The deceleration of droplets (from $51\,m/s$ to $30\,m/s$) looks not so drastic at a glance; however, it becomes quite prominent ($555\,g$) as estimated in Table 4, should the elapsed time of droplet transition per the distance be considered. It evokes again the fact that small droplets with small inertia are prone to lose quickly their momentum to surrounding air.

IV. $C_{L,DW}$ vs. $C_{H,DW}$: The considerable deceleration of droplets under the higher injection pressure resulted in a little lower mean velocity than under the lower injection pressure. At these downstream positions, atomization is matured regardless of the level of injection pressure.

The above interpretation for four situations could be also applied to the other injector nozzle orifices, taking into account the distributional similarity of instantaneous data as well as the variational behavior of their mean values.

An appropriate categorization for atomization and turbulence nature can be made accounting for a spray
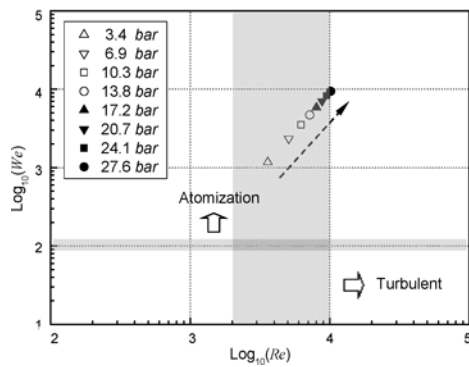
Fig. 14. Categorization of spray-flow regime by the interrelation of jet Reynolds number and Weber number.

Fig. 15. Effect of injection pressure on the variation of droplet number density for *Nozzle Orifice* #2 spray.

regime interrelating the jet Reynolds number *Re* with Weber number *We*, as shown in Fig. 14. Both dimensionless parameters are defined as follows, employing the injection velocity at the orifice exit $V_{inj,\bar{C}_d}$ as was given in Fig. 10:

$$Re = \frac{\rho_w V_{inj,\bar{C}_d} d}{\mu_w} \qquad (3)$$

$$We = \frac{\rho_w V_{inj,\bar{C}_d}^2 d}{\sigma_w} \qquad (4)$$

Generally accepted are the spray regimes identified in the figure: jet flow becomes turbulent where $Re > 2 \times 10^3$ through 1×10^4 assuming it is uniform and free of oscillations, and atomization begins where $We > 1 \times 10^2$ [3]. It is found that all the cases considered in prior description pertain to highly probable atomization regime while their turbulence nature transits into fully turbulent region only as the injection pressure goes up. Increasing Weber number necessarily results in the enhancement of atomization capability: considering the Weber number implying an index for the inertial force to surface tension acting on a fluid element, sprays under the high injection pressure condition with augmented kinetic energy are highly prone to be atomized.

The more atomized spray results in the more spreading in the instantaneous velocity of droplets because of the dynamic randomness of smaller droplets. Those characteristics can be authenticated from an investigation about the variation of turbulent intensity as well as number density of droplets. It is clearly shown in Fig. 15 that the number density increases as the injection pressure does, but on the other hand
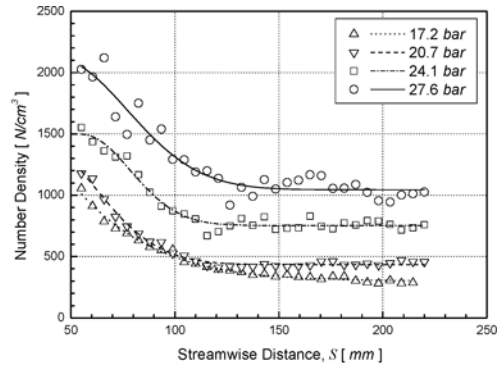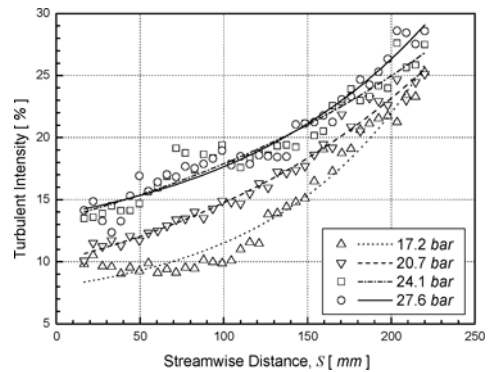

Fig. 16. Enhancement of droplet turbulent-intensities along the spray stream with the injection pressure increase for the *Nozzle Orifice* #3.

decreases along with spray evolution toward downstream: the former indicates the greater atomization at the elevated pressure, and the latter is a direct outcome of the spray-angle widening. Fig. 16 reveals that turbulent intensities of droplets are enhanced with the pressure augmentation and as moving toward downstream as well, which Jung et al. [26] reported in detail in their previous study.

A spray evolution with breakup process is schematized in Fig. 17, where the scrutiny made through the frozen images captured by FVS setup and the velocity/size of droplets measured by DPDA has been conceptually reflected. With an overlapped shedding feature that could be glanced through the images, the schematic has been slightly modified on the basis of the illustrations of Baumgarten et al. [27] and Stiesch [28]. Spray evolution in the present experiment may be categorized largely into two regimes of primary break-up (from the nozzle orifice exit up to 60.5 *mm*, approximately) and secondary break-up (further
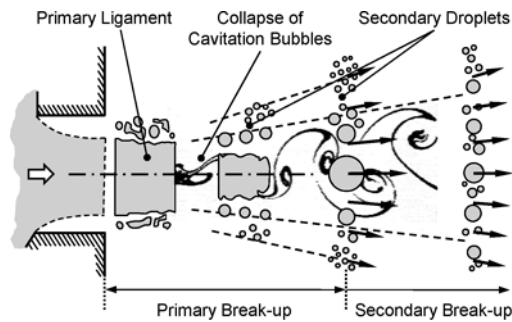
Fig. 17. Schematization of spray evolution with break-up.

downstream thereafter). Again, the primary break-up regime is subdivided into the regions of primary ligament (approximately to 16.5 *mm* away from orifice exit) and secondary droplets, and a region in between where liquid ligament and secondary droplets coexist.

4. Conclusions

Spray characteristics for the injector of a full scale and direct injection type employed in a 5 Newton-class of liquid-propellant thruster have been addressed with the evolutionary features of droplets. Instantaneous images were captured by CCD camera of FVS setup, and droplet information was obtainable through DPDA measurement in terms of the velocity, diameter, number density, and turbulent intensity. Especially, a rationale for the DPDA-velocity measurement accuracy was established based on the volume flow rate directly measured in the experiment.

Throughout the investigation of instantaneous spray images, the thruster injector under consideration was demonstrated to meet an angular injection requirement at all pressure levels endowed. With the supplement of video-microscope images for the orifice inlet configuration, a concern of the inter-orifices inconsistency associated with EDM-fabrication was also raised by examining dissimilarity among the sprays emanating from a set of nozzle orifices in an injector. Spray shedding, which may be interrelated with flow instabilities, was obtainable by skeletonizing the frozen spray images.

Dynamic behavior and atomization evolution of spray droplets along the spray stream on an axis of nozzle orifice with varying injection pressures were scrutinized through the changing feature of droplet velocities and sizes with the aid of cumulative population of droplets mapped onto the velocity-diameter domain, and further

authenticated on the basis of the distribution for number density and turbulent intensity of droplets. It has been inferred to the droplet dynamics in the current type of injector sprays that (1) the deceleration of droplets traveling through surrounding air strongly depends upon the degree of atomization, which is proportional to the injection pressure, (2) the diminishing rate of AMD along the spray stream shrinks as the injection pressure goes up, and (3) the higher injection pressure generates the smaller droplets undergoing the greater decrease rate of velocity along the spray stream, with both of the (1) and (2) features being concurrently considered. There has been also found through a spray regime categorization that all the sprays under the pressures considered pertain to highly probable atomization regime while their turbulence nature transits into fully turbulent region only as the injection pressure goes up.

Characterization of the sprays in the current type of thruster injector has never been made before. It is expected that the present results and ensuing study will be able to contribute to the design engineering of a brand-new thruster as well as to the greater comprehension for performance features of the thrusters in use.

Nomenclature————————————————

AMD : Arithmetic mean diameter
C   : *Cases* combining injection pressure and probing location
C_d : Discharge coefficient
$\bar{C}_d$: Averaged discharge coefficient
d   : Diameter, nozzle orifice
l   : Length, nozzle orifice
P   : Pressure
$\dot{Q}$: Volume flow rate
Re   : Reynolds number
S   : Distance along the orifice axis
V   : Velocity
We   : Weber number

Greek symbols

δ : Dimension in fringe volume
μ : Viscosity
ρ : Density

σ : Surface tension

Subscript

atm : Atmosphere
DPDA : Dual-mode phase Doppler anemometry
DW : Downstream
H : High (pressure)
inj : Injection
inlet : Nozzle orifice inlet
L : Low (pressure)
UP : Upstream
w : Liquid water
x, y, z : Coordinate system in measurement

References

[1] J. S. Kim, J. Park, S. Kim, J. Choi and K. W. Jang, Test and performance evaluation of small liquid-monopropellant rocket engines, *42nd AIAA/ASME/ SAE/ASEE Joint Propulsion Conference and Exhibit*, (2006) AIAA-2006-4388.

[2] K. Miller, J. Sisco, N. Nugent and W. Anderson, Combustion instability with a single-element swirl injector, *Journal of Propulsion and Power*, 23 (5) (2007) 1102-1112.

[3] R. J. Kenny, M. D. Moser, J. Hulka and G. Jones, Cold flow testing for liquid propellant rocket injector scaling and throttling, *42nd AIAA/ASME/SAE/ ASEE Joint Propulsion Conference and Exhibit*, (2006) AIAA-2006-4705.

[4] X. Li and J. Shen, Experimental study of sprays from annular liquid jet breakup, *Journal of Propulsion and Power*, 15 (1) (1999) 103-110.

[5] J. Y. Koo, The effects of injector nozzle geometry and operating pressure conditions on the transient fuel spray behavior, *KSME International Journal*, 17 (3) (2003) 617-625.

[6] R. Payri, S. Molina, F. J. Salvador and J. Gimeno, A study of the relation between nozzle geometry, internal flow and sprays characteristics in Diesel fuel injection systems, *KSME International Journal*, 18 (7) (2004) 1222-1235.

[7] R. D. Reitz and F. V. Bracco, Mechanism of atomization of a liquid jet, *Physics of Fluids*, 25 (10) (1982) 1730-1742.

[8] C. F. Edwards and K. D. Marx, Analysis of the ideal phase-Doppler system: limitations imposed by the single-particle constraint, *Atomization & Sprays*, 2 (3) (1992) 319-366.

[9] M. Saffman, The use of polarized light for optical particle sizing, *Proc. of 3rd International Symposium on Applications of Laser Anemometry to Fluid Mechanics*, Lisbon, Portugal, (1986) 387-398.

[10] G. Gréhan, G. Gouesbet, A. Naqwi and F. Durst, Evaluation of a phase Doppler system using generalized Lorenz-Mie theory, *Proc. of International Conference on Multiphase Flows*, Tsukuba, Japan, (1991) 291-294.

[11] S. V. Sankar, A. Inenaga and W. D. Bachalo, Trajectory dependent scattering in phase Doppler interferometry: minimizing and eliminating sizing errors, *Proc. of 6th International Symposium on Applications of Laser Techniques to Fluid Mechanics*, Lisbon, Portugal, (1992) Paper 12.2.

[12] J. Domnick, V. Dorfner, F. Durst and M. Yamashita, Performance evaluation of different phase-Doppler systems, *Particle & Particle Systems Characterization*, 11 (1) (1994) 91-100.

[13] C. Tropea, T. H. Xu, F. Onofri, G. Gréhan and P. Haugen, Dual-mode phase Doppler anemometry, *Proc. of 7th International Symposium on Applications of Laser Techniques to Fluid Mechanics*, Lisbon, Portugal, (1994) Paper 18.3.

[14] J. S. Kim, J. S. Kim, H. Jung, J. Park, S. Kim and K. W. Jang, A study on the spray characteristics of a liquid-propellant thruster injector by PIV/PDA optical measurements, *5th Joint ASME/JSME Fluids Engineering Conference*, (2007) FEDSM2007-37105.

[15] E. W. Schmidt, *Hydrazine and Its Derivatives: Preparation, Properties, Applications, 2nd Ed. John Wiley & Sons Inc.*, New York, USA, (2001).

[16] C. Tropea, T. H. Xu, F. Onofri, G. Gréhan, P. Haugen and M. Stieglmeier, Dual-mode phase-Doppler anemometer, *Particle & Particle Systems Characterization*, 13 (2) (1996) 165-170.

[17] A. H. Lefebvre, *Atomization and Sprays, Hemisphere Publishing Corp.*, New York, (1989).

[18] L. C. Ganippa, G. Bark, S. Andersson and J. Chomiak, Cavitation: a contributory factor in the transition from symmetric to asymmetric jets in cross-flow nozzles, *Experiments in Fluids*, 36 (4) (2004) 627-634.

[19] H. Hiroyasu, Spray break-up mechanism from the hole-type nozzle and its applications, *Atomization and Sprays*, 10 (3-5) (2000) 511-527.

[20] T. Tamaki, M. Shimizu, K. Nishida and H. Hiroyasu, Effects of cavitation and internal flow on atomization of a liquid jet, *Atomization and Sprays*, 8 (2) (1998) 179-197.

[21] M. Kato, H. Kano, K. Date, T. Oya and K. Niizuma, Flow analysis in nozzle hole in consideration of cavitation, (1997) *SAE Paper* 970052.

[22] J. Lee, S. Kang and B. Rho, Intermittent atomization characteristics of multi-hole and single-hole Diesel nozzle, *KSME International Journal*, 16 (12) (2002) 1693-1701.

[23] Z. Faragó and N. Chigier, Morphological classification of disintegration of round liquid jets in a coaxial air stream, *Atomization and Sprays*, 2 (2) (1992) 137-153.

[24] J. H. Im, M. K. Kim and Y. Yoon, Self-pulsation characteristics of a swirl injector, *10th International Congress on Liquid Atomization and Spray Systems*, Kyoto, Japan, (2006) ICLASS06-092.

[25] B. J. Azzopardi, Measurement of drop sizes, *International Journal of Heat and Mass Transfer*, 22 (9) (1979) 1245-1279.

[26] H. Jung, J. S. Kim, S. Kim and J. Park, Effects of fuel-injection pressure on the spray breakup characteristics in small LRE injector, *Journal of the Korean Society of Propulsion Engineers*, 11 (3) (2007) 50-57.

[27] C. Baumgarten, J. Stegemann and G. P. Merker, A new model for cavitation induced primary break-up of Diesel sprays, *Proc. of 18th ILASS Europe Conference*, Zaragoza, Spain, (2002) 15-20.

[28] G. Stiesch, *Modeling Engine Spray and Combustion Processes, Springer-Verlag NY Inc.*, New York, (2003).

Jin Seok Kim obtained his B.S. and M.S. degrees in Mechanical Engineering in 2005 and 2007, respectively, from Sunchon National University, Korea. He is currently a Ph.D. candidate.

Jeong Soo Kim took his master's and Ph.D. degrees in Aerospace Engineering in 1987 and 1992, respectively from KAIST, Korea. Since then, he worked for Agency for Defense Development and Korea Aerospace Research Institute as a principal researcher up to 2004. Also he researched at TRW (USA) as an assistant program manager from 1996 to 1998. He is currently a faculty member in the School of Mechanical Engineering of Pukyong National University, Korea. His research fields extend into the development of space propulsion engines with their components design, T&E of liquid rocket engines, and the numerical simulation of combustion phenomena.